Received: 15 March 2022 | Revised: 25 May 2022 | Accepted: 6 June 2022

DOI: 10.1002/aic.17805

AIChE JOURNAL

RESEARCH ARTICLE

Thermodynamics and Molecular-Scale Phenomena

What does the NRTL model look like? Determination of boundaries for different fluid phase equilibrium regions

Juan A. Labarta | María M. Olaya | Antonio F. Marcilla

Department of Chemical Engineering, Institute of Chemical Process Engineering, University of Alicante, Alicante, Spain

Correspondence
Juan A. Labarta, Department of Chemical Engineering, Institute of Chemical Process Engineering, University of Alicante, PO 99, Alicante E-03080, Spain.
Email: ja.labarta@ua.es

Abstract

The adequate correlation of experimental phase equilibrium data by using any thermodynamic model represents a key point for the rigorous design of the chemical processes. However, this data correlation process remains a challenging problem, due to the high nonlinearity of the models used and the consequent problems of convergence. The present work analyzes the nonrandom two-liquids mode (NRTL) model to check the relation between the values of the binary interaction parameters and the corresponding phase equilibria that the NRTL model can or cannot reproduce. Additionally, in the case of the LLE, empirical equations have been established as a function of the nonrandomness parameter, to model the trajectory of the different miscibility boundaries observed. These functions can be used as constraints in the experimental data correlation procedure to reduce the search space and guarantee the consistency of the obtained binary interaction parameters with the experimental behavior of the system under study.

KEYWORDS
experimental data correlation, Gibbs energy of mixing, LLE, miscibility boundaries, NRTL model, phase equilibria, VLE

1 | INTRODUCTION

Nowadays, chemical engineers are fully focused on developing more efficient and sustainable separation processes, regarding process systems engineering and process-product design. The use of computer-aided process engineering is essential to reach this goal. The current computational capacity allows calculating hundreds of simulations to obtain the optimal design of the separation process under study, in a relatively short time, considering not only the economic point of view, but also the corresponding environmental impacts associated using multiobjective optimization (MOO) techniques, life cycle assessment, sustainable profits, and so on. All these simulations and optimal designs can be done in different ways:

- Using commercial chemical process simulators[1] such as Aspen-Plus®, Aspen-Hysys®, or ChemCad®.
- Using classical or extended tray by tray methods for instance in the case of reactive distillation,[2] quaternary liquid–liquid extractors,[3] or internally heat-integrated distillation columns.[4]
- Using specific optimization algorithms based on generalized disjunctive programming or stochastic programming to optimize from single equipment to complex superstructures regarding, for example, distillation or extraction sequences,[5–7] water pretreatment networks,[8] and so on.
- Or even using hybrid proposals that combine the advantages of the previous alternatives.[9–14]

In any case, the precision of any approach to modeling and reproducing any separation process will largely depend on the consistency and quality of the model used, and its parameters, to correctly predict and represent the corresponding phase equilibria. There are several examples of the current relevance of this topic. For instance, the thermodynamic modeling of mixtures with new solvents such as ionic liquids (cataloged as more environmentally friendly solvents due to their low volatilities) that present high selectivity and normally complex equilibrium behaviors,[15–18] with interest also as bio-solvents and cell disrupting agents[19] Other relevant examples, are the development of new and more sustainable continuous pharmaceutical manufacturing processes,[20] where the optimal design of liquid–liquid extraction cascades is required, the design of advanced distillation process (as extractive distillations), or new CO_2 capture procedures, both using ionic liquids.[21,22]

In this context, as has been pointed out previously,[23–25] the correlation of the experimental equilibrium data to obtain the corresponding parameters of any model to reproduce that phase equilibria is a nontrivial issue, and it is not exempt from mathematical problems associated with the high nonlinearly and non-convexity of the equations used. All these problems generate strong convergence difficulties, dependence on the starting strategy used, and the presence of local optima. For these reasons, it is especially necessary to double-check the total consistency of the behavior and the quality of the phase equilibria that the model predicts (with the parameters obtained in the correlation process), regarding the experimental behavior of the system under study in the whole range of compositions (not only around the experimental data used).

To avoid all these difficulties when correlating experimental data from different kinds of phase equilibria, including liquid–liquid equilibrium (LLE), vapor–liquid equilibrium (VLE), liquid–liquid–liquid equilibrium (LLLE), liquid–solid equilibrium (LSE), liquid–liquid–solid equilibrium (LLSE), and so on, different approaches have been published over the years. For instance, analyzing the own limitations of the models such as the existence of gaps in the nonrandom two-liquids mode (NRTL) model where solutions for binary homogeneous liquid behavior do not exist[26] or considering higher temperature or pressure dependence in the binary interaction parameters when it is required.[27–29] It is also possible to find different mathematical strategies[30–35] and algorithms based on the Gibbs energy of mixing (G^M),[36–42] for improving the convergence and robustness of phase equilibria calculations in complex systems. These alternatives normally include topological strategies for the selection of more adequate supposed phase equilibrium compositions (to start the correlation process) or for the confirmation of the consistency of the correlation results, for example, in the case of LLE for ternary systems with three partially miscible binary subsystems (type 3) including a three-liquid-phase region. Specific mathematical restrictions quite useful have also been developed and applied successfully[43–45] in the thermodynamic modeling of type 0 (island), type 1, and 2 systems, for systems that had not been previously adjusted using the NRTL model or presented in the literature correlation results inconsistent with the experimental behavior of the system. Additionally, different extensions of classical models, such as the NRTL model, can also be found for complex LLE[44] or VLE,[46–49] and non-azeotropic or azeotropic VLLE.[50–52]

In the present article, a deep analysis of the NRTL model has been carried out, studying the existence of different liquid–liquid (LL) and vapor–liquid (VL) equilibrium regions and boundaries in the space defined by its binary interaction parameters, for obtaining a clear picture of this model, its possibilities and flexibility. In this sense, the different boundaries observed in the case of the LLE have been mathematically modeled, with the final aim of obtaining relationships between the binary interaction parameters that can be used as constraints for avoiding directly inconsistent results with the experimental behavior of the system under study, when the NRTL model is used in the correlation of experimental equilibrium data.

Therefore, the main objective of the present work is to help researchers and engineers, that need to deal with the task of correlating experimental phase equilibrium data, to obtain consistent binary interaction parameters, in this case for the NRTL model, that nowadays still being one of the most used models to calculate phase equilibria in the optimal design or rigorous simulation of chemical process or equipment. Unfortunately, it is important to remark at this point that parameters of thermodynamic models (such as NRTL and UNIQUAC) that are inconsistent with the experimental behavior that is intended to be correlated are still being published.

Thus, the article is organized as follows: in Section 2, the NRTL equation and its flexibility are briefly revised. In Section 3, binary spinodal surfaces and LLE maps have been calculated with the NRTL model for different values of the nonrandomness parameter. Next, the correlation of the boundaries detected, by using empirical equations, is presented and formulated as constraints using generalized disjunctive representations. In Section 5, the VLE is analyzed by representing the corresponding phase equilibrium maps of NRTL binary interaction parameters and checking all the different phase equilibrium behaviors found (including different azeotropic behaviors) remarking that, in this case, the maps obtained also depend on the vapor pressure of the pure components. Finally, the main conclusions of the present study are summarized.

2 | NRTL EQUATION

The NRTL model[53] is still one of the most widely used models to calculate the equilibrium between phases in multicomponent systems, including totally miscible or partially miscible liquid mixtures. The NRTL equation for the Gibbs energy of excess for the liquid phase is the following:

$$\frac{G^{E,L(NRTL)}}{RT} \equiv g^{E,L(NRTL)} = \sum_{i=1}^{n}\left(x_i \cdot \frac{\sum_{j=1}^{n}\left(\tau_{j,i}\cdot G_{j,i}\cdot x_j\right)}{\sum_{l=1}^{n}\left(G_{l,i}\cdot x_{l,i}\right)}\right)$$
$$\text{where: } \tau_{j,i} = \frac{1}{T}\cdot\frac{g_{j,i}-g_{i,i}}{R} = \frac{A_{j,i}}{T} \qquad (1)$$
$$G_{j,i} = \exp\left(-\alpha_{j,i}\cdot\tau_{j,i}\right)$$

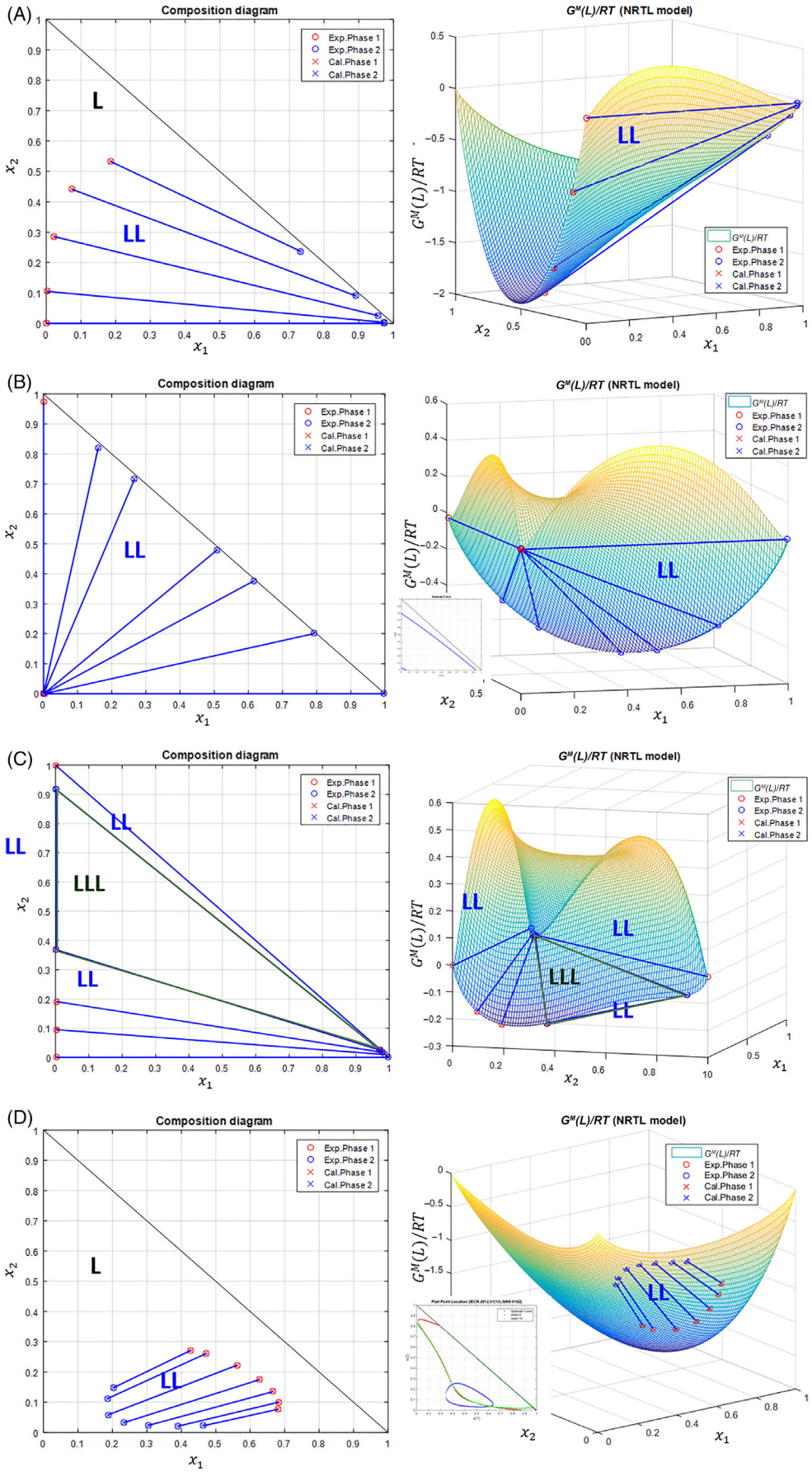

FIGURE 1 Examples of the flexibility of the NRTL model to generate different LLE behaviors (Treybal classification[54]): (A) type 1, (B) type 2, (C) type 3, and (D) type 0

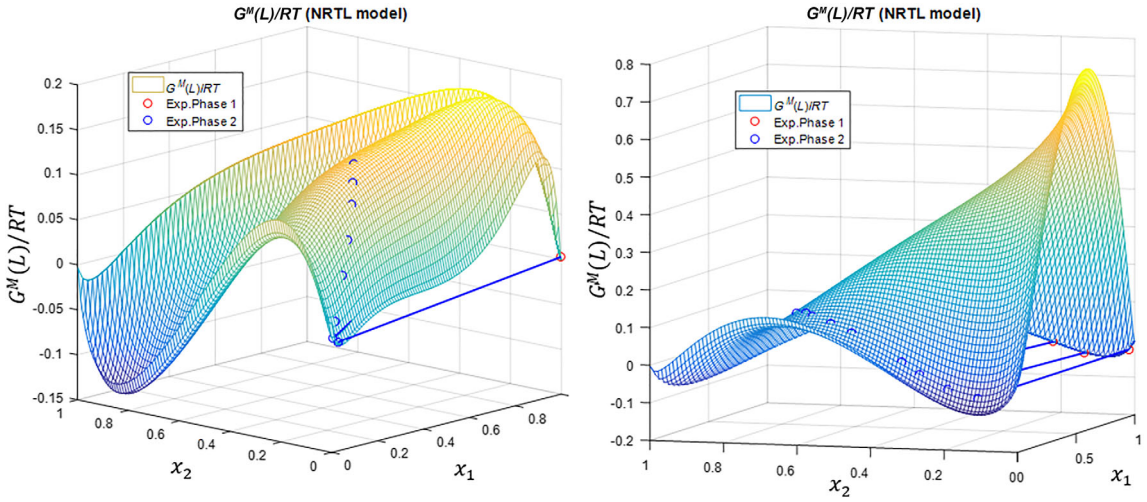

FIGURE 2 Examples of inconsistent results in experimental data correlations (analyzing the whole range of compositions). Calculated $G^M(L)/RT$ surfaces and initial experimental LLE tie-lines correlated

where n represents the number of components of the mixture. As it is possible to observe, this equation only contains binary interaction parameters where $g_{j,i}$ is a characteristic energetic parameter for the binary interaction between the components j–i. $\alpha_{j,i} = \alpha_{i,j}$ is a positive parameter related to the nonrandom distribution of the mixture and it will only be zero for completely random mixtures.

With this expression, the NRTL equation can reproduce a large amount of VL and LL equilibrium behaviors. Figure 1 shows the composition diagram and Gibbs Energy of Mixing function (Equation 2) as examples of the flexibility of the NRTL model[55,56] for reproducing the different types of LLE following the Treybal classification.[54] In the case of type 2 and 0 systems, the analysis of the Hessian Matrix (spinodal curve)[45] is also included to confirm the typology of the system.

$$\frac{G^{M,L(NRTL)}}{RT} = \frac{G^{ideal,L}}{RT} + \frac{G^{E,L(NRTL)}}{RT} = \sum_{i=1}^{n} x_i \cdot ln(x_i) + \frac{G^{E,L(NRTL)}}{RT} \quad (2)$$

However, despite the flexibility shown to reproduce complex behaviors, as mentioned earlier in the introduction section, certain precautions must be taken when using the NRTL model, as with any other model, to correlate experimental equilibrium data. On the one hand, that a model presents great flexibility in general, does not mean that it cannot additionally present certain specific limitations.[26–28] On the other hand, it is always necessary to double-check if the solution obtained in the experimental data correlation process is totally consistent with the experimental behavior of the system under study, analyzing the entire range of compositions.[23–25,29,35] In this sense, Figure 2 shows two examples of Gibbs mixing energy surfaces calculated from recently published NRTL binary interaction parameters obtained by correlation of ternary LL experimental data, which, however, are inconsistent with the experimental behavior of the studied system when the whole range of compositions is analyzed (not only the tie lines used in the correlation process). In both cases, the system under study corresponds to a type 1 system, but the calculated Gibbs mixing energy surface shows that all the binary subsystems are heterogeneous (corresponding therefore to a type 3 system) and that there exists additionally a tie triangle with three liquids in equilibrium.

3 | NRTL LLE MAPS: BINARY SPINODAL SURFACES AND MISCIBILITY BOUNDARIES

In a previous article,[57] two different equilibrium regions (and the corresponding boundary) were detected when representing the dimensionless conjugated binary interaction parameters $\tau_{i,j}$ and $\tau_{j,i}$, (with $\alpha_{i,j} = 0.2$) of the NRTL model, for 300 systems obtained from DECHEMA Data Collection.[58] In order to check in a first step the dependence of this miscibility boundary on the nonrandomness parameter ($\alpha_{i,j}$), a set of different equilibrium maps in the $\tau_{i,j}$–$\tau_{j,i}$–x_i space, for different values of $\alpha_{i,j}$ from 0 to 0.95 has been generated by discrete scanning.

Although the use of values of 0.2 and 0.3 can produce very good results in an important number of examples, there are also a large number of published cases where these values cannot generate the expected experimental behavior. This is the case for instance of several ionic liquids that presents huge binodal curves, or a strong variation of the slope of the tie-lines, and so on. Additionally, although there may be some specific cases with values of $\alpha_{i,j}$ greater than 1, for example in the case of some VLE data[58] such as the systems water + phenol, water + 6-caprolactam, or 2-butanone + phenol correlated with $\alpha_{i,j}$ values of 1.196, 5.297, and 6.557, respectively, the immense majority of the fluid phase equilibria correlated with the NRTL model present values of $\alpha_{i,j}$ lower than one.

The possibility of the existence of LLE phase splitting has been analyzed through zeros of the second derivative (inflection points) of the Gibbs energy of mixing function (respect to mole fraction), for each set of $\tau_{i,j}$–$\tau_{j,i}$ values, in the whole composition range ($x_i \in [0,1]$).

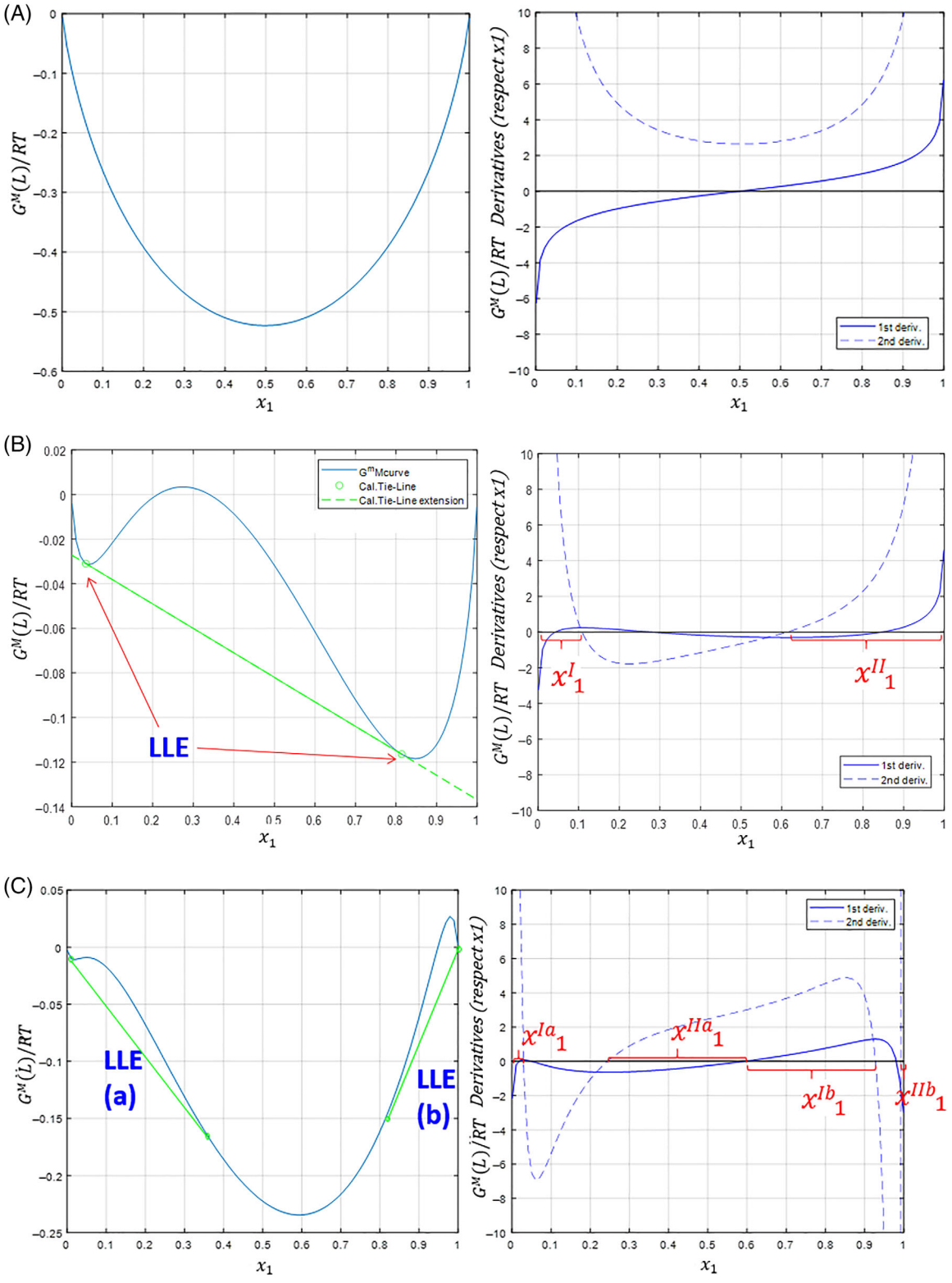

FIGURE 3 Representation of the Gibbs energy of mixing function curve and its first and second derivatives for different situations: (A) a homogeneous liquid, (B) one LLE splitting ($x^I{}_1$–$x^{II}{}_1$), and (C) two LLE splits ($x^{Ia}{}_1$–$x^{IIa}{}_1$ and $x^{Ib}{}_1$–$x^{IIb}{}_1$)

Figure 3 shows the Gibbs energy of mixing function and its derivatives for different examples. Figure 3A represents the situation for a homogeneous liquid where the second derivative of the Gibbs energy of mixing function does not present any zero, while Figure 3B shows the case of a LL splitting, where the second derivative of the Gibbs energy of mixing function presents two zeros. The location of these zeros in

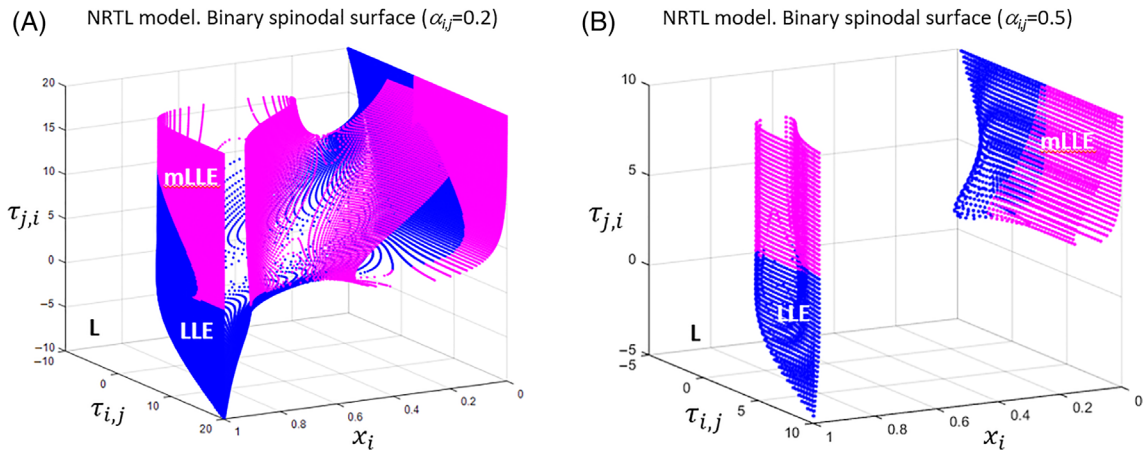

FIGURE 4 3D representation of the binary spinodal surface of the NRTL model for $\alpha_{i,j}$ values of (A) 0.2 and (B) 0.5

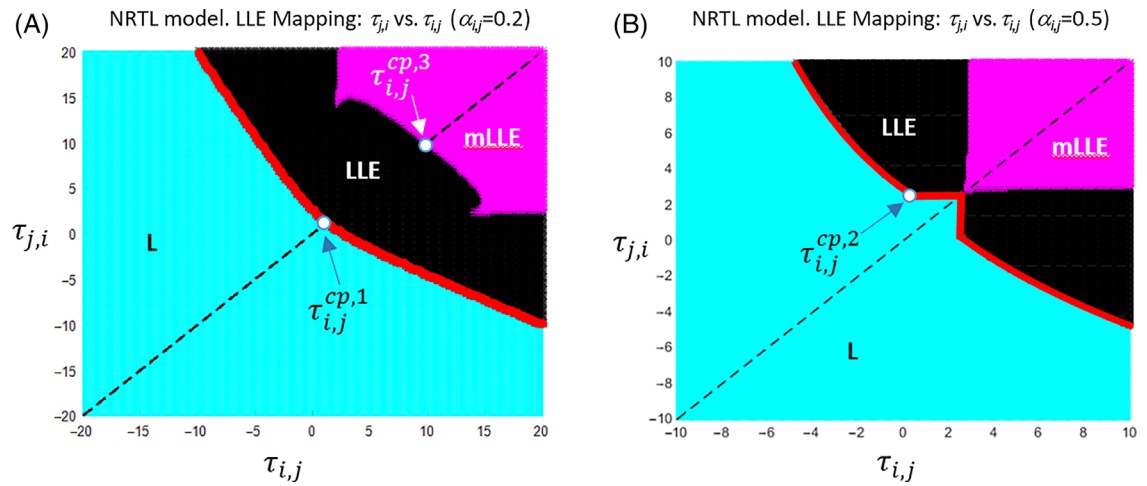

FIGURE 5 $\tau_{j,i}$ vs. $\tau_{i,j}$ LL equilibrium map for the NRTL model dependent on the value $\alpha_{i,j}$. (A) $\alpha_{i,j} = 0.2$, (B) $\alpha_{i,j} = 0.5$

the ordinate axis allows defining upper and lower bounds for the calculated equilibrium compositions. Thus, in this example, the molar fraction of the two liquid phases in equilibrium (x^{I}_1 and x^{II}_1) would be located, as a first approximation, in the ranges (0.0, 0.109) and (0.614, 1.0), respectively. Finally, Figure 3C shows a case where two different LLE splits (x^{Ia}_1–x^{IIa}_1 and x^{Ib}_1–x^{IIb}_1) are possible in the whole range of compositions.

In this sense, Figure 4A shows the $\tau_{i,j}$–$\tau_{j,i}$–x_i 3D map corresponding to the $\alpha_{i,j}$ value of 0.2, used normally in the correlation of experimental LLE data. The axes of this graph correspond to the mole fraction of one component (*i*), and the dimensionless binary interaction parameters $\tau_{i,j}$ and $\tau_{j,i}$, respectively. The plotted points represent the combination of the variables x_i, $\tau_{i,j}$, and $\tau_{j,i}$ where the corresponding second derivative of the Gibbs energy of mixing is equal to zero, that is, this series of inflection points represents a kind of binary spinodal surface in this 3D space. The points in dark blue represent the combinations of $\tau_{i,j}$ and $\tau_{j,i}$ parameters that present only one LL splitting in the whole range of compositions (e.g., Figure 3B). On the other hand, the points marked in light pink indicate the presence of more than one LLE (mLLE) for the corresponding combination of $\tau_{i,j}$ and $\tau_{j,i}$ parameters, because there are more than two compositions that present a value of zero in the second derivative of the Gibbs energy of mixing (e.g., Figure 3C). The rest of the space corresponds to homogeneous liquid mixtures (*L*). As it can be observed, there exists spinodal (inflection) points (and therefore, LL splitting) distributed in the whole range of $\tau_{j,i}$–$\tau_{i,j}$–x_i values. Only for extreme values of $\tau_{j,i}$–$\tau_{i,j}$, higher than 10 and lower than −5, respectively, these spinodal points are located in a narrow range of compositions near the pure components.

Additionally, Figure 4B represents the situation for $\alpha_{i,j} = 0.5$. In this case, it can be noticed that the location of most of the spinodal points is near to the pure components, and therefore there exist a large range of compositions where no liquid–liquid equilibrium can be predicted. This situation is even more remarkable for higher values of $\alpha_{i,j}$.

Figure 5 shows the projection of these spinodal surfaces (for $\alpha_{i,j}$ values of 0.2 and 0.5) on the $\tau_{i,j}$–$\tau_{j,i}$ plane. These projections generate interesting 2D graphs where two regions are differentiated, as well as the corresponding miscibility boundaries. The bisector of the first and

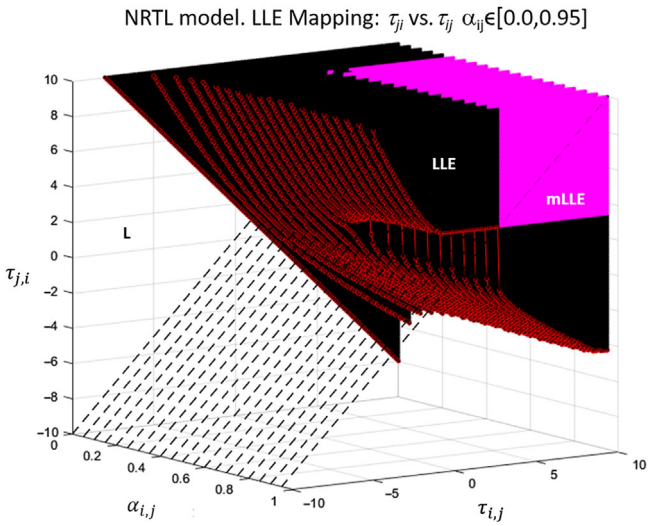

FIGURE 6 $\tau_{j,i}$ vs. $\tau_{i,j}$ LL equilibrium maps for the NRTL model ($\alpha_{i,j} \in [0.0, 0.95]$)

third quadrant has been included as an auxiliary line. The light cyan blue region (*L*) below the boundary (red curve) corresponds to the region where no LL splitting exits, that is, the liquid homogeneous region. On the other hand, the zone above the boundary represents the liquid heterogeneous region, and two different sub-regions can be observed. One sub-region that includes all the combinations of $\tau_{i,j}$–$\tau_{j,i}$ values that present only one LLE splitting (the black one), and another sub-region at high values of the $\tau_{i,j}$ or $\tau_{j,i}$ parameters showing multiple LLE splits (mLLE). The border between the L and LLE regions in Figure 5A represents the miscibility boundary previously found[57] for the NRTL model for $\alpha_{i,j} = 0.2$. Figure 5B corresponds to the situation for $\alpha_{i,j} = 0.5$. It is possible to observe how, in this case, the miscibility boundary suffers significant changes and evolves to intersect the mLLE region over the first and third quadrant bisector. Additionally, it is possible to see that if we use the value of 10 as the upper bound for $\tau_{j,i}$, in both cases, the miscibility boundary exists in the range of values of $\tau_{i,j}$ from -5 to 10. At this point, it is also important to remark the symmetric behavior that these figures present with the bisector of the first and third quadrant (dotted line) and some characteristic change points ($\tau_{i,}^{p,k}$) that we will explore in the next sections.

If we extend this analysis to a larger range of $\alpha_{i,j}$ values, it is possible to obtain the complete 3D map represented in Figure 6 (in the Supporting Information all the individual graphics for $\alpha_{i,j}$ from 0 to 0.95 can be found). In this figure, we can see how the LLE miscibility boundary starting from a straight line at $\alpha_{i,j} = 0$, remains a smooth curve until an $\alpha_{i,j}$ value of 0.4. After this value, when increasing the value of $\alpha_{i,j}$, the boundary curve begins to show a progressive distortion that ends with the intersection of the miscibility boundary with the mLLE region (over the plotted bisector) at $\alpha_{i,j} = 0.43$ and higher. The mLLE region appears approximately from $\alpha_{i,j} = 0.15$ onward and includes in some cases metastable LLE solutions (e.g., when the corresponding G^M curve presents two local maximum and a global minimum). To help the direct visualization of all these charts and calculations, in a similar way to the previous graphical user interface (GUI) developed to systematically check the consistency of LLE or LVE data correlation results,[29,56] a new GUI, also publicly available online, has been created in the MatLab® software. This Boundaries_LL_NRTL GUI[59] allows to visualize and calculate, for the NRTL model, all the previous LL equilibrium maps and miscibility boundaries, and also to generate a grid with individual Gibbs energy of mixing curves in the whole range of composition, for a set of pairs τ_{ij}–τ_{ji} tested in the corresponding discrete scanning (see also Figure S2A–D).

4 | CORRELATION OF THE MISCIBILITY BOUNDARIES DETECTED

In order to mathematically model the previous NRTL miscibility boundaries and their dependence on the nonrandomness parameter ($\alpha_{i,j}$), the following empirical equation has been used, where the different coefficients p_q depend on the $\alpha_{i,j}$ value:

$$\tau_{j,i}^{\text{boundary,cal}} = f_{\text{boundary}}(\tau_{ij}, \alpha_{ij}) = p_1 \cdot \tau_{ij}^3 + p_2 \cdot \tau_{ij}^2 + p_3 \cdot \tau_{ij} + p_4 \quad (3)$$

$$p_q = a_q + b_q \cdot \ln(\alpha_{ij} + c_q) + d_q \cdot \alpha_{ij} + e_q \cdot \alpha_{ij}^2 \quad q = \{1,2,3,4\} \quad (4)$$

Note that the parameter c_q is needed to include, in the correlation process, the miscibility boundary corresponding to $\alpha_{i,j} = 0$, otherwise, this parameter would be unnecessary.

Taking advantage of the symmetry observed in the miscibility boundaries, only the first smooth boundary sections above the bisector of the 1st and 3rd quadrants (until the point we will denominate change point: $\tau_{i,j}^{cp,k}$, see Figure 5) have been simultaneously correlated for different $\alpha_{i,j}$ values. Thus, in order to carry out the correlation process, different sets of boundaries have been defined. The first group includes all the L–LLE miscibility boundaries (those from $\alpha_{i,j} = 0$ to $\alpha_{i,j} = 0.4$) that are quite smooth in the whole range of existence, for example, from $\tau_{i,j} = -10$ to $\tau_{i,j} = 10$. In this case, $\tau_{i,j}^{cp,1}$ corresponds with the intersection of the boundary with the mentioned bisector (Figure 5A). The second group includes a set of L–LLE boundaries for $\alpha_{i,j}$ values higher than 0.4 and that present a change point, $\tau_{i,j}^{cp,2}$, before the intersection with the bisector (Figure 5B). Regarding the LLE–mLLE boundaries, there exist also two different behaviors as commented before. The first group of LLE–mLLE boundaries for $\alpha_{i,j}$ between 0.15 and 0.43 that present a smooth curve starting approximately at $\tau_{i,j} = 2.21$, with a change point $\tau_{i,j}^{cp,3}$ (Figure 5A), which corresponds with the intersection of the LLE–mLLE boundary with the 1st and 3rd quadrants bisector. The second group of LLE–mLLE boundaries from $\alpha_{i,j} = 0.43$ to $\alpha_{i,j} = 0.95$ corresponds to straight lines starting from the bisector. As it is possible to observe in Figure 5B, this second group of LLE–mLLE boundaries also intersects with the corresponding L–LLE miscibility boundary.

The location on the abscissa axis of the change points $\tau_{i,j}^{cp,k}$ (Figure 5) for each group of boundaries (k = 1, 2, 3) has been correlated using a polynomial equation of order three: $g_k(\alpha_{i,j})$:

$$\tau_{i,j}^{cp,k} \equiv g_k(\alpha_{ij}) = t_{1,k} \cdot \alpha_{ij}^3 + t_{2,k} \cdot \alpha_{ij}^2 + t_{3,k} \cdot \alpha_{ij} + t_{4,k} \quad (5)$$

TABLE 1 Parameters of Equations (3) and (4) obtained from the simultaneous fitting of the different L–LLE miscibility boundaries: f_{LLE} ($\tau_{i,j}$, $\alpha_{i,j}$) with $\alpha_{i,j}$ from 0.0 to 0.95

f_{LLE} ($\tau_{i,j}$,$\alpha_{i,j}$) p_q:	p_1	p_2	p_3	p_4
a_q	0.17018	0.94122	−15.8026	7.41426
b_q	1.18745	0.38618	6.61230	8.99112
c_q	0.86617	0.08518	9.30456	0.54484
d_q	−1.29669	−2.15462	−2.06603	−11.2860
e_q	0.45992	1.95455	3.08991	3.68998

Note: *RDS(%)* = 0.03 ($N = 1755$ and $P = 20$).

After that, the different equilibrium boundaries have been correlated simultaneously for different values of $\alpha_{i,j}$ using Equations (3) and (4). In the case of the L–LLE boundaries, both boundary groups have been simultaneously correlated with the same set of parameters of Equations (3) and (4), for 29 values of $\alpha_{i,j}$ between 0 and 0.95 (both included). In the case of the observed boundary curves between the LLE and mLLE regions in the range of $\alpha_{i,j}$ values from 0.15 to 0.43, the parameters c_q are equal to zero, because the value $\alpha_{i,j} = 0$ is not included in the simultaneous correlation of this set of boundaries.

Tables 1–3 show all the parameters obtained in the simultaneous correlation. The quality of the correlations has been quantified by using the relative standard deviation or variation coefficient:

$$RSD(\%) = \left| \frac{\sqrt{\sum_{r=1}^{N} \left(\tau_{j,i}^{\text{boundary,cal},r} - \tau_{j,i}^{\text{boundary},r}\right)^2 / (N-P)}}{\sum_{r=1}^{N} \tau_{j,i}^{\text{boundary},r} / N} \right| \cdot 100 \qquad (6)$$

where N is the total number of correlated points, P is the number of parameters to be fitted, $\tau_{i,j}^{\text{boundary,cal},r}$ corresponds to the calculated values from the proposed Equations (1) and (2) for each boundary point r, and $\tau_{i,j}^{\text{boundary},r}$, represents the original boundary value obtained from the corresponding NRTL equilibrium map (e.g., Figure 6).

Finally, Figure 7 shows the evolution of the calculated L–LLE and LLE–mLLE boundaries in the range of $\alpha_{i,j}$ values studied, to visualize their main general characteristics. This figure represents the trajectories of the calculated $\tau_{j,i}$ vs. $\tau_{i,j}$ boundaries (L–LL and LL–mLL) obtained for the different values of the $\alpha_{i,j}$ parameter, in consonance with the behavior of these boundaries described in previous sections.

5 | MATHEMATICAL FORMULATION OF THE MISCIBILITY BOUNDARY CONSTRAINTS

To take advantage of the previous characterization and modeling of the existing NRTL miscibility boundaries and their dependence on the $\alpha_{i,j}$ values, and thus be able to directly avoid inconsistent results when dealing with an experimental data correlation problem, the following formulation is proposed. This approach allows including all the knowledge about the miscibility boundaries in any calculation algorithm, as a way to restrict the feasible searching space of the corresponding binary interaction parameters. Thus, using a generalized disjunctive representation, the constraint corresponding to a binary subsystem with a liquid homogeneous phase (located below the corresponding L–LLE miscibility boundary) could be formulated as follows:

$$\begin{bmatrix} \alpha_{i,j} \in [0,0.4] \\ \begin{bmatrix} \tau_{i,j} \in \left[-10, \tau_{i,j}^{cp,1}\right] \\ \tau_{j,i} - f_{LLE}\left(\tau_{i,j}, \alpha_{i,j}\right) < 0 \end{bmatrix} \vee \begin{bmatrix} \tau_{i,j} \in \left(\tau_{i,j}^{cp,1}, 10\right] \\ \tau_{i,j} - f_{LLE}\left(\tau_{j,i}, \alpha_{i,j}\right) < 0 \end{bmatrix} \end{bmatrix} \vee \begin{bmatrix} \alpha_{i,j} \in [0.4,0.95] \\ \begin{bmatrix} \tau_{i,j} \in \left[-5, \tau_{i,j}^{cp,2}\right] \\ \tau_{j,i} - f_{LLE}\left(\tau_{i,j}, \alpha_{i,j}\right) < 0 \end{bmatrix} \vee \begin{bmatrix} \tau_{i,j} \in \left(\tau_{i,j}^{cp,2}, f_{LLE}\left(\tau_{i,j}^{cp,2}, \alpha_{i,j}\right)\right] \\ \tau_{j,i} - f_{LLE}\left(\tau_{i,j}^{cp,2}, \alpha_{i,j}\right) < 0 \end{bmatrix} \vee \begin{bmatrix} \tau_{i,j} \in \left(f_{LLE}\left(\tau_{i,j}^{cp,2}, \alpha_{i,j}\right), 10\right] \\ \tau_{i,j} - f_{LLE}\left(\tau_{j,i}, \alpha_{i,j}\right) < 0 \end{bmatrix} \end{bmatrix} \qquad (7)$$

The disjunctions included in Equation (7), first divide the two different behaviors observed in the LLE boundary with the $\alpha_{i,j}$ values, that is, in the ranges [0, 0.4] and (0.4, 0.95]. Inside each of these intervals, it has been used the shape and symmetry that presents the corresponding boundary, as it has been analyzed in Section 3, using the location of the changing points, $\tau_{i,j}^{cp,k}$, defined in Section 4 and Figure 5. Thus, to use the obtained equation (f_{LLE}) below the bisector of the first and third quadrant, a change in the order of the components *i* and *j*, in the binary interaction parameters, has to be done.

In the case of a heterogeneous binary subsystem presenting two liquid phases in equilibrium, two constraints could be used for the corresponding correlation data. The first one, by simply changing the sense of the zero inequalities at each disjunction of Equation 7, because the heterogeneous equilibria are located above the L–LLE miscibility boundary, and a second constraint (Equation 9) to avoid the mLLE region (e.g., Figure 5A,B):

TABLE 2 Parameters of Equations (3) and (4) obtained from the simultaneous fitting of the different LLE–mLLE boundaries: $f_{mLLE}(\tau_{i,j}, \alpha_{i,j})$ with $\alpha_{i,j}$ from 0.15 to 0.43

$f_{mLLE}(\tau_{i,j},\alpha_{i,j})$ p_q:	p_1	p_2	p_3	p_4
a_q	0.17970	3.66704	−12.2321	−169.867
b_q	0.04713	1.09335	−2.70716	−78.5291
d_q	−1.00726	−11.9808	66.6629	299.304
e_q	2.93938	0.38653	−69.0533	−146.868

Note: *RDS(%)* = 0.03 ($N = 1755$ and $P = 20$).

TABLE 3 Parameters of the polynomial equations $g_k(\alpha_{i,j})$ used to correlate the different selected changing points $\tau_{i,j}^{cp,k}$ ($P = 4$)

Boundary	*k*	$\alpha_{i,j}$	$t_{1,k}$	$t_{2,k}$	$t_{3,k}$	$t_{4,k}$	*N*	*RDS* (%)
L–LLE	1	[0,0.4]	11.0599	−7.61356	2.78799	0.94847	14	0.03
	2	[0.4,0.95]	−18.9354	46.0735	−37.9180	10.6231	16	5.51
LLE–mLLE	3	[0.15,0.43]	−712.144	769.320	−297.731	44.5980	13	0.47

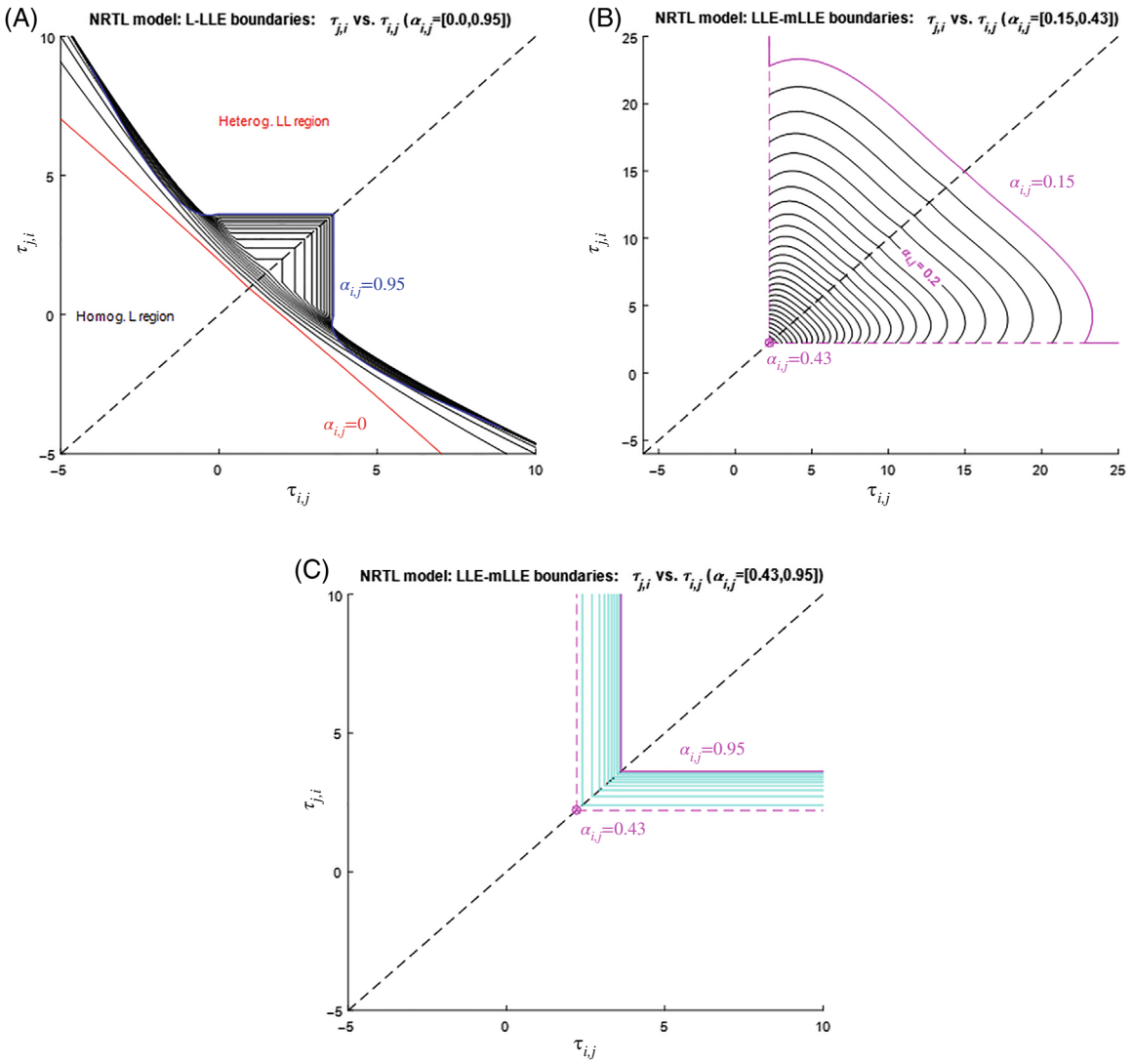

FIGURE 7 Calculated $\tau_{j,i}$ vs. $\tau_{i,j}$ miscibility boundaries for the NRTL model: (A) L–LLE boundaries ($\alpha_{i,j} \in [0.0, 0.95]$); (B) LLE–mLLE boundaries ($\alpha_{i,j} \in [0.15, 0.43]$); (C) LLE–mLLE boundaries ($\alpha_{i,j} \in [0.43, 0.95]$)

$$\begin{bmatrix} \alpha_{i,j} \in [0,0.4] \\ \begin{bmatrix} \tau_{i,j} \in \left[-10, \tau_{i,j}^{cp,1}\right] \\ \tau_{j,i} - f_{LLE}\left(\tau_{i,j}, \alpha_{i,j}\right) > 0 \end{bmatrix} \vee \begin{bmatrix} \tau_{i,j} \in \left(\tau_{i,j}^{cp,1}, 10\right] \\ \tau_{i,j} - f_{LLE}\left(\tau_{j,i}, \alpha_{i,j}\right) > 0 \end{bmatrix} \end{bmatrix}$$

$$\vee \tag{8}$$

$$\begin{bmatrix} \alpha_{i,j} \in [0.4,0.95] \\ \begin{bmatrix} \tau_{i,j} \in \left[-5, \tau_{i,j}^{cp,2}\right] \\ \tau_{j,i} - f_{LLE}\left(\tau_{i,j}, \alpha_{i,j}\right) > 0 \end{bmatrix} \vee \begin{bmatrix} \tau_{i,j} \in \left(\tau_{i,j}^{cp,2}, f_{LLE}\left(\tau_{i,j}^{cp,2}, \alpha_{i,j}\right)\right] \\ \tau_{j,i} - f_{LLE}\left(\tau_{i,j}^{cp,2}, \alpha_{i,j}\right) > 0 \end{bmatrix} \vee \begin{bmatrix} \tau_{i,j} \in \left(f_{LLE}\left(\tau_{i,j}^{cp,2}, \alpha_{i,j}\right), 10\right] \\ \tau_{i,j} - f_{LLE}\left(\tau_{j,i}, \alpha_{i,j}\right) > 0 \end{bmatrix} \end{bmatrix}$$

$$\begin{bmatrix} \alpha_{i,j} \in [0.15,0.43) \\ \tau_{i,j} \in \left[2.21, \tau_{i,j}^{cp,3}\right] \\ \tau_{j,i} - f_{mLLE}\left(\tau_{i,j}, \alpha_{i,j}\right) < 0 \end{bmatrix} \vee \begin{bmatrix} \alpha_{i,j} \in [0.15,0.43) \\ \tau_{i,j} \in \left(\tau_{i,j}^{cp,3}, f_{mLLE}\left(2.21, \alpha_{i,j}\right)\right] \\ \tau_{i,j} - f_{mLLE}\left(\tau_{j,i}, \alpha_{i,j}\right) < 0 \end{bmatrix} \vee \begin{bmatrix} \alpha_{i,j} \in [0.43,0.95) \\ \tau_{i,j} \in \left[f_{LLE}\left(\tau_{i,j}^{cp,2}, \alpha_{i,j}\right), 10\right] \\ \tau_{j,i} - f_{LLE}\left(\tau_{i,j}^{cp,2}, \alpha_{i,j}\right) < 0 \end{bmatrix} \tag{9}$$

Obviously, for the case of a binary subsystem with mLLE, the constraint would be:

$$\begin{bmatrix} \alpha_{i,j} \in [0.15,0.43) \\ \tau_{i,j} \in \left[2.21, \tau_{i,j}^{cp,3}\right] \\ \tau_{j,i} - f_{mLLE}\left(\tau_{i,j}, \alpha_{i,j}\right) > 0 \end{bmatrix} \vee \begin{bmatrix} \alpha_{i,j} \in [0.15,0.43) \\ \tau_{i,j} \in \left(\tau_{i,j}^{cp,3}, f_{mLLE}\left(2.21, \alpha_{i,j}\right)\right] \\ \tau_{i,j} - f_{mLLE}\left(\tau_{j,i}, \alpha_{i,j}\right) > 0 \end{bmatrix} \vee \begin{bmatrix} \alpha_{i,j} \in [0.43,0.95) \\ \tau_{i,j} \in \left[f_{LLE}\left(\tau_{i,j}^{cp,2}, \alpha_{i,j}\right), 10\right] \\ \tau_{j,i} - f_{LLE}\left(\tau_{i,j}^{cp,2}, \alpha_{i,j}\right) > 0 \end{bmatrix} \tag{10}$$

The mathematical application of the previous constraints can be done directly in the case of using any spreadsheet (such as Microsoft Excel and its solver toolbox) for the correlation calculations.[60–63] In the case of using a specific optimization software such as GAMS,[64] the previous disjunctions could be reformulated as an MINLP model by using the Big M reformulation or the general hull reformulation in the case of nonlinear equations.[65,66]

6 | MAPPING NRTL BINARY VAPOR–LIQUID EQUILIBRIA REGIONS

The previous analysis can be applied in the same way to the case of the binary vapor–liquid equilibria, including different azeotropic behaviors. One important difference in the case of VLE is that the equilibrium maps, in the range of binary interaction parameters studied, depend additionally on the vapor pressure of the pure components selected, through the corresponding parameters of the equation used (e.g., Antoine's Equation).

Figure 8 shows, as an example, the results obtained for a system where the boiling temperatures of the pure components are around:

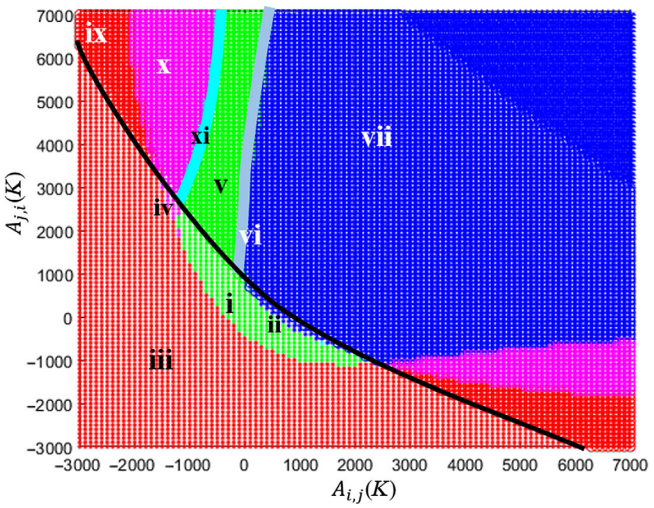

FIGURE 8 $A_{j,i}$ vs. $A_{i,j}$ VL equilibrium map for the NRTL model with $\alpha_{i,j} = 0.2$ at atmospheric pressure. Antoine's parameters: $A_1 = 6.9547$; $B_1 = 1170.97$, $C_1 = 226.232$, $A_2 = 8.0713$, $B_2 = 1730.63$, and $C_2 = 233.426$. T_{ref} to check additionally possible LLE = 56°C

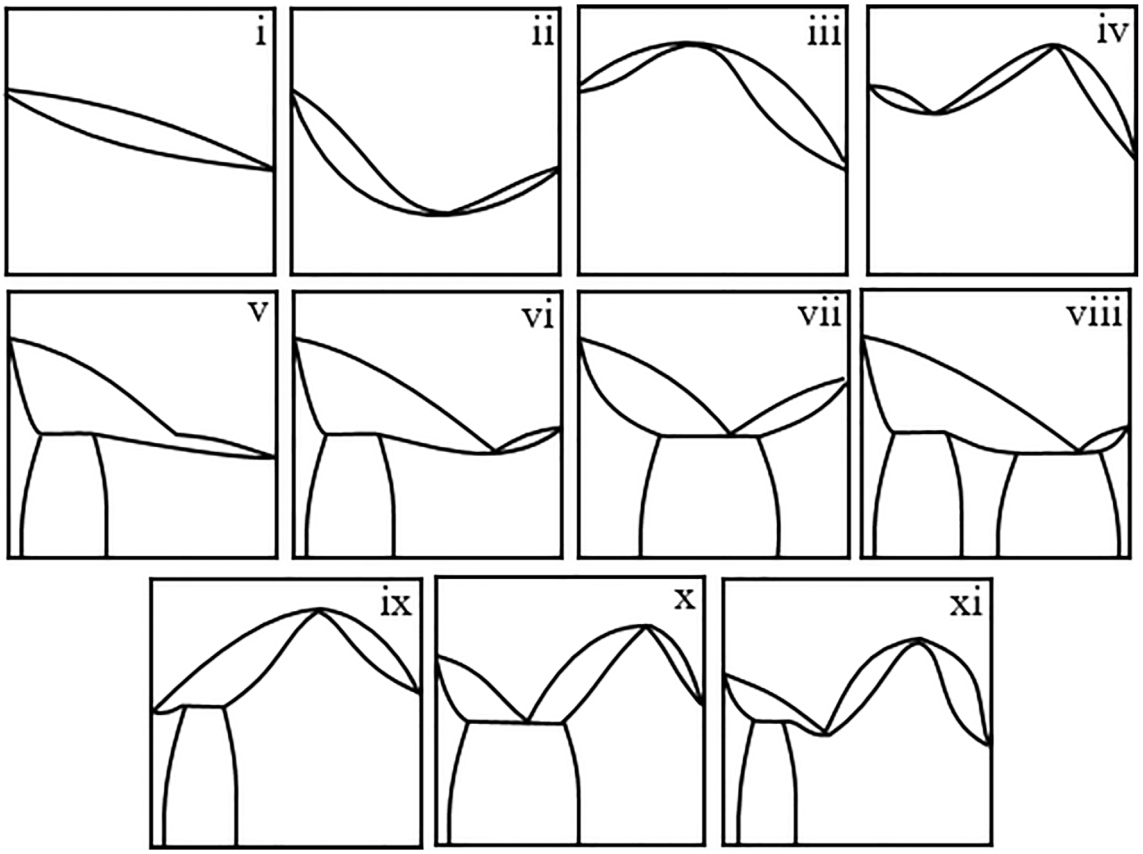

FIGURE 9 Qualitative temperature-composition diagrams (*T* vs. x, y) for the different VL equilibrium behaviors observed

60 and 100°C, in the matrix of binary interaction parameters analyzed (within a range including the typical values observed in DECHEMA). Different phase equilibrium regions[67] and the transition between them can be observed, dependent on the values of the binary interaction parameters of the NRTL equation. Note that in this case, the $A_{i,j}$ binary interaction parameters have been used instead of the $\tau_{i,j}$ parameters to exclude the effect of the temperatures in the parameters, taking into account that in this case, each point of the equilibrium map has a different temperature. The L–LL miscibility boundary has also been included to facilitate the visualization of homogeneous and heterogeneous liquid regions. Thus, it is possible to observe how depending on the $A_{i,j}$ values, different phase equilibrium behaviors can be obtained such as:

In the homogeneous liquid region:

i. VLE without azeotropes.
ii. VLE with a homogeneous VL minimum boiling temperature azeotrope.
iii. VLE with a homogeneous VL maximum boiling point azeotrope.
iv. VLE with two homogeneous azeotropes, one minimum boiling point azeotrope and one maximum boiling point azeotrope.

In the LL heterogeneous region:

v. LLE and VLE without azeotropes.
vi. LLE and VLE with one (homogeneous) minimum boiling point azeotrope.
vii. VLLE with a heterogeneous azeotrope.
viii. VLLE with two different LLE including one heterogeneous azeotrope.
ix. LLE and VLE with one (homogeneous) maximum boiling point azeotrope.
x. VLLE with one heterogeneous azeotrope and one homogeneous maximum boiling point azeotrope.
xi. LLE and VLE with two homogeneous azeotropes, one minimum boiling point azeotrope and one maximum boiling point azeotrope.

Figure 9 represents the qualitative temperature-composition diagrams of the different phase equilibrium behaviors observed. In any case, the size and evolution of these regions depend on the boiling temperatures of the pure components studied. In general, the regions without azeotropes increase with the difference in these temperatures, decreasing the regions with homogeneous and heterogeneous azeotropes. In the Supporting Information, the calculated maps for different sets of Antonie's parameters have been included.

7 | CONCLUSIONS

The existing boundaries for different phase equilibrium regions, using the NRTL model, have been analyzed by representing the corresponding equilibrium maps of binary interaction parameters, for the case of LLE and VLE, in this last case with 11 different regions, including different kinds of homogeneous and heterogeneous azeotropes, and with sizes that depend on the vapor pressure of the pure components. For the case of the LLE and its experimental data correlation problem, a set of equations have been developed to model, in the $\tau_{j,i}$–$\tau_{i,j}$ space, the trajectory of all the different L–LL and LL–mLL miscibility boundaries observed in the present work, which depend on the nonrandomness parameter ($\alpha_{i,j}$). Additionally, different mathematical constraints have been formulated, in order to reduce the corresponding search space (depending on the characteristics of the experimental system under study), and helping not only the convergence of the calculations, but also avoid the possibility of finding solutions inconsistent with the experimental behavior of the equilibrium studied. A GUI (publicly available online) has also been created to easily view all the spinodal surfaces and miscibility boundaries analyzed and modeled.

In this sense, future works will include the theoretical definition and calculation of the boundaries for different equilibrium behavior regions previously observed, by analyzing the Gibbs energy of mixing function and its corresponding second and third derivatives.

Finally, to conclude, the knowledge and characterization of the different types of phase equilibrium behaviors, in relation to the corresponding binary interaction parameters, can be of great interest in the binary interaction parameter optimization when correlating experimental phase equilibrium data, to establish consistent initial points for the optimization algorithm, and therefore in the posterior use of these parameters in the simulation or optimal design of the process and/or equipment related.

AUTHOR CONTRIBUTIONS

Juan A. Labarta: Conceptualization (equal); data curation (lead); formal analysis (lead); investigation (equal); methodology (equal); software (lead); supervision (equal); validation (equal); visualization (lead); writing – original draft (lead); writing – review and editing (equal). **María M. Olaya:** Validation (equal); writing – review and editing (equal). **Antonio Marcilla:** Conceptualization (equal); investigation (equal); methodology (equal); validation (equal); writing – review and editing (equal).

DATA AVAILABILITY STATEMENT

Data available in article Supporting Information.

NOMENCLATURE

A_{ij}	binary interaction parameters (*K*) for components *i,j*
A_i,B_i,C_i	parameters of Antoine's equation for component *i*
a_q,b_q,c_q,d_q,e_q	parameters of the equation used for the calculation of p_q as a function of $\alpha_{i,j}$
$\alpha_{i,j}$	nonrandomness NRTL factor
$G^{E,L}$, $g^{E,L}$	excess Gibbs energy of the liquid phase (J mol^{-1} and dimensionless, respectively)
$G^{\text{idea},L}$	ideal Gibbs energy of mixing of the liquid phase (J mol^{-1})
$G^{M,L}$	Gibbs energy of mixing of the liquid phase (J mol^{-1})
$g_{j,i}$	characteristic energetic parameter for the binary interaction between the components *j–i*
$G_{j,i}$	NRTL parameter dependent on $\alpha_{i,j}$ and $\tau_{i,j}$ (Equation 1)
GUI	graphical user interface
mLLE	multiple liquid–liquid equilibria
N	total number of correlated miscibility boundary points (*r*)
n	number of components
NRTL	nonrandom two-liquids model
LLE	liquid–liquid equilibrium
LLLE	liquid–liquid–liquid equilibrium
LSE	liquid–solid equilibrium
LLSE	liquid–liquid–solid equilibrium
P	number of parameters to be fitted
p_q	Parameters dependent on $\alpha_{i,j}$ used for correlating the observed NRTL miscibility boundaries with $q = \{1, 2, 3, 4\}$
R	universal gas constant
RSD	relative standard deviation or variation coefficient
T	temperature (K)
τ_{ij}	binary interaction parameters (dimensionless) for components *i,j*
$\tau_{i,}^{\text{boundary}}$	binary interaction parameters (dimensionless) for components *i,j* in the corresponding miscibility boundary, obtained from the corresponding NRTL equilibrium map (e.g., Figure 5)
$\tau_{i,}^{\text{boundary,cal}} = f_{\text{boundary}}(\tau_{i,j},\alpha_{i,j})$	binary interaction parameters (dimensionless) for components *i,j* in the corresponding miscibility boundary, calculated from the proposed Equations (1) and (2)
$\tau_{i,}^{cp,k} = g_k(\alpha_{i,j})$	characteristic change points (dependent on $\alpha_{i,j}$) used to take advantage of the symmetric behavior presented by the observed boundaries with the bisector of the first and third quadrant ($k = \{1, 2, 3\}$, Figure 5)
T_{ref}	reference temperature used in the VLE calculations to check additionally possible LLE
VLE	vapor–liquid equilibrium
x_i	liquid molar fraction of component *i*
x^F_i	equilibrium molar fraction of component *i* in liquid phase *F*

Superscripts

cal	calculated value
L	liquid phase
r	miscibility boundary point

Subscripts

i, j, l	components

ORCID

Juan A. Labarta https://orcid.org/0000-0002-4870-2031

REFERENCES

1. Seader JD, Henley EJ, Roper DK. *Separation Process Principles With Applications Using Process Simulators*. 4th ed. John Wiley & Sons, Inc; 2016.
2. Lee JW, Hauan S, Lien KM, Westerberg AW. A graphical method for designing reactive distillation columns: I. The Ponchon–Savarit method. *Proc R Soc A: Math Phys Eng Sci*. 2000;456:1953-1964.
3. Marcilla A, Gómez A, Reyes JA, Olaya MM. New method for quaternary systems liquid-liquid extraction tray to tray design. *Ind Eng Chem Res*. 1999;38(8):3083-3095.
4. Ho TJ, Huang CT, Lee LS, Chen CT. Extended Ponchon-Savarit method for graphically analyzing and designing internally heat-integrated distillation columns. *Ind Eng Chem Res*. 2010;49:350-358.
5. Caballero JA, Grossmann IE. Generalized disjunctive programming model for the optimal synthesis of thermally linked distillation columns. *Ind Eng Chem Res*. 2001;40(10):2260-2274.
6. Leboreiro J, Acevedo J. Processes synthesis and design of distillation sequences using modular simulators: a genetic algorithm framework. *Comput Chem Eng*. 2004;28(8):1223-1236.
7. Reyes-Labarta JA, Grossmann IE. Disjunctive optimisation design models for complex liquid-liquid multistage extractors. *AIChE J*. 2001;47(10):2243-2252.
8. Carrero-Parreño A, Onishi V, Salcedo-Diaz R, et al. Optimal pretreatment system of flowback water from shale gas production. *Ind Eng Chem Res*. 2017;56:4386-4398.
9. Caballero JA, Milan-Yanez D, Grossmann IE. Rigorous design of distillation columns: integration of disjunctive programming and process simulators. *Ind Eng Chem Res*. 2005;44(17):6760-6775.
10. Odjo AO, Sammons NE Jr, Yuan W, Marcilla A, Eden MR, Caballero JA. Disjunctive-genetic programming approach to synthesis of process networks. *Ind Eng Chem Res*. 2011;50:6213-6228.
11. Brunet R, Reyes-Labarta JA, Guillén-Gosálbez G, Jiménez L, Boer D. Combined simulation-optimization methodology for the design of environmental conscious absorption systems. *Comput Chem Eng*. 2012;46:205-216.
12. Labarta JA, Caballero JA, Marcilla A. A novel hybrid simulation-optimization approach for the optimal design of multicomponent distillation columns. *Comp-Aided Chem Eng*. 2012;30:1257-1261.
13. Javaloyes-Antón J, Ruiz-Femenia R, Caballero JA. Rigorous design of complex distillation columns using process simulators and the Particle Swarm Optimization Algorithm. *Ind Eng Chem Res*. 2013;52:15621-15634.
14. Kong L, Maravelias CT. From graphical to model-based distillation column design: a McCabe-Thiele-inspired mathematical programming approach. *AIChE J*. 2019;65:e16731. doi:10.1002/aic.16731
15. Rodríguez-Escontrela I, Arce A, Soto A, Marcilla A, Olaya MM, Reyes-Labarta JA. Correlation of three-liquid-phase equilibria involving ionic liquids. *Phys Chem Chem Phys*. 2016;18:21610-21617.
16. Wen G, Bai W, Zheng F, et al. Ternary liquid-liquid equilibrium of an azeotropic mixture (hexane + methanol) with different imidazolium-based ionic liquids at T = 298.15 K and 101.325 kPa. *Fluid Phase Equilib*. 2018;461:51-56.
17. Wang P, Yan P, Reyes-Labarta JA, et al. Liquid-liquid measurement and correlation for separation of azeotrope (dimethyl carbonate and ethanol) with different imidazolium-based ionic liquids. *Fluid Phase Equilib*. 2019;485:183-189.
18. Zhu Z, Xu Y, Feng T, et al. Measurement and correlation of liquid–liquid equilibria of three imidazolium ionic liquids with acetone and cyclohexane. *J Mol Liq*. 2020;298:111947-111962.
19. Mussagy CU, Santos-Ebinuma VC, Gonzalez-Miquel M, Coutinho JAP, Pereira JFB. Protic ionic liquids as cell disrupting agents for the recovery of intracellular carotenoids from yeast Rhodotorula glutinis CCT-2186. *ACS Sustainable Chem Eng*. 2019;7:16765-16776.
20. Diab S, Gerogiorgis DI. Technoeconomic mixed integer nonlinear programming (MINLP) optimization for design of liquid-liquid extraction (LLE) cascades in continuous pharmaceutical manufacturing of atropine. *AIChE J*. 2019;65:e16738. doi:10.1002/aic.16738
21. Diao B, Wang Z, Yang H, et al. Separation of azeotrope 2,2,3,3-tetrafluoro-1-propanol and water by extractive distillation using ionic liquids: vapor-liquid equilibrium measurements and interaction analysis. *J Mol Liq*. 2019;292:111424-111432.
22. Qazi S, Gómez-Coma L, Albo J, Druon-Bocquet S, Irabien A, Sanchez-Marcano J. CO_2 capture in a hollow fiber membrane contactor coupled with ionic liquid: influence of membrane wetting and process parameters. *Sep Purif Technol*. 2020;233:115986.
23. Marcilla A, Reyes-Labarta JA, Olaya MM. Should we trust all the published LLE correlation parameters in phase equilibria? Necessity of their assessment prior to publication. *Fluid Phase Equilib*. 2017;433:243-252.
24. Marcilla A, Olaya MM, Reyes-Labarta JA. Ensuring that correlation parameters for liquid−liquid equilibrium produce the right results (Editorial). *J Chem Eng Data*. 2018;63(5):1133-1134.
25. Bazyleva A, Abildskov J, Anderko A, et al. Good reporting practice for thermophysical and thermochemical property measurements (IUPAC Technical Report). *Pure Appl Chem*. 2021;93(2):253-272.
26. Marcilla A, Olaya MM, Serrano MD, Reyes-Labarta JA. Methods for improving models for condensed phase equilibrium calculations. *Fluid Phase Equilib*. 2010;296:15-24.
27. Marcilla A, Olaya MM, Reyes-Labarta JA. The unavoidable necessity of considering temperature dependence of the liquid Gibbs energy of mixing for certain VLE data correlations. *Fluid Phase Equilib*. 2018;473:17-31.
28. Marcilla A, Olaya MM, Reyes-Labarta JA, Carbonell-Hermida P. Procedure for the correlation of normal appearance VLE data, where the classical models dramatically fail with no apparent reason. *Fluid Phase Equilib*. 2019;493:88-101.
29. Labarta JA, Olaya MM, Marcilla A. GMcal_TieLinesLV: graphical user interface (GUI) for the topological analysis of GM functions for binary and ternary (isobaric or isothermal) vapor-liquid equilibrium (VLE) data (including tie-lines, derivatives, Distillation Boundaries etc.). Institutional Repository of the University of Alicante (RUA). 2022. http://hdl.handle.net/10045/122857.
30. Castillo J, Grossmann IE. Computation of phase and chemical equilibria. *Comput Chem Eng*. 1981;5:99-108.
31. McDonald CM, Floudas CA. Global optimization for the phase and chemical equilibrium problem: application to the NRTL equation. *Comput Chem Eng*. 1995;19(11):1111-1139.
32. Mitsos A, Bollas GM, Barton PI. Bilevel optimization formulation for parameter estimation in liquid–liquid phase equilibrium problems. *Chem Eng Sci*. 2009;64:548-559.
33. Bollas GM, Barton PI, Mitsos A. Bilevel optimization formulation for parameter estimation in vapor-liquid(−liquid) phase equilibrium problems. *Chem Eng Sci*. 2009;64:1768-1783.
34. Voskov AL, Dzuban AV, Maksimov AL. TernAPI program for the calculation of ternary phase diagrams with isolated miscibility gaps by the convex hull method. *Fluid Phase Equilib*. 2015;388:50-58.
35. Glass M, Aigner M, Viell J, Jupke A, Mitsos A. Liquid-liquid equilibrium of 2-methyltetrahydrofuran/water over wide temperature range: measurements and rigorous regression. *Fluid Phase Equilib*. 2017;433:212-225.

36. Reyes JA, Conesa JA, Marcilla A, Olaya MM. Solid-liquid equilibrium thermodynamics: checking stability in multiphase systems using Gibbs energy function. *Ind Eng Chem Res*. 2001;40:902-907.
37. Olaya MM, Marcilla A, Serrano MD, Botella A, Reyes-Labarta JA. Simultaneous correlation of LL, LS and LLS equilibrium data for water + organic solvent + salt ternary systems. Anhydrous solid phase. *Ind Eng Chem Res*. 2007;46(21):7030-7037.
38. Olaya MM, Ibarra I, Reyes-Labarta JA, Serrano MD, Marcilla A. Computing liquid-liquid phase equilibria: an exercise to understand the nature of false solutions and how to avoid them. *Chem Eng Edu*. 2007;41(3):218-224.
39. Marcilla A, Reyes-Labarta JA, Olaya MM, Serrano MD. Simultaneous correlation of liquid-liquid, liquid-solid, and liquid-liquid-solid equilibrium data for water + organic solvent + salt ternary systems: hydrated solid phase formation. *Ind Eng Chem Res*. 2008;47:2100-2108.
40. Marcilla A, Olaya MM, Serrano MD, Velasco R, Reyes-Labarta JA. Gibbs energy based procedure for the correlation of type 3 systems including a three-liquid phase region. *Fluid Phase Equilib*. 2008;278:87-95.
41. Labarta JA, Olaya MM, Velasco R, Serrano MD, Marcilla A. Correlation of the liquid-liquid equilibrium data for specific ternary systems with one or two partially miscible binary subsystems. *Fluid Phase Equilib*. 2009;281:9-14.
42. Díaz I, Rodríguez M, González EJ, González-Miquel M. A simple and reliable procedure to accurately estimate NRTL interaction parameters from liquid-liquid equilibrium data. *Chem Eng Sci*. 2019;193:370-378.
43. Olaya MM, Reyes-Labarta JA, Velasco R, Ibarra I, Marcilla A. Modelling liquid-liquid equilibria for Island type ternary systems. *Fluid Phase Equilib*. 2008;265(1–2):184-191.
44. Marcilla A, Olaya MM, Serrano MD, Reyes-Labarta JA. Aspects to be considered for the development of a correlation algorithm for condensed phase equilibrium data of ternary systems. *Ind Eng Chem Res*. 2010;49(20):10100-10110.
45. Marcilla A, Serrano MD, Reyes-Labarta JA, Olaya MM. Checking liquid-liquid critical point conditions and their application in ternary systems. *Ind Eng Chem Res*. 2012;51(13):5098-5102.
46. Seyf JY, Shojaeian A. Vapor-liquid (azeotropic systems) and liquid-liquid equilibrium calculations using UNIFAC and NRTL-SAC activity coefficient models. *Fluid Phase Equilib*. 2019;494:33-34.
47. Agarwal NK, Mondal BK, Samanta AN. Measurement of vapour-liquid equilibrium and e-NRTL model development of CO_2 absorption in aqueous dipropylenetriamine. *Environ Sci Pollut Res*. 2021;28:19285-19297.
48. Urdaneta MR. Using the NRTL model with the vidal equation of state EOS-qE formulation for vapor/liquid equilibrium calculations. *Fluid Phase Equilib*. 2014;365:123-132.
49. Ma Y, Gao J, Xu D, Zhang L, Wang Y. Vapor-liquid equilibrium study of binary mixtures of chloroform, 2-ethylhexanoic acid, and propylene glycol methyl ether at atmospheric pressure. *J Chem Eng Data*. 2020;65:2271-2279.
50. Steltenpohl P, Graczová E. Application of extended NRTL equation for ternary liquid–liquid and vapor–liquid–liquid equilibria description. *Chem Pap*. 2010;64(3):310-317.
51. Marcilla A, Olaya MM, Reyes-Labarta JA. Simultaneous VLLE data correlation for ternary systems: modification of the NRTL equation for improved calculations. *Fluid Phase Equilib*. 2016;426:47-55.
52. Marcilla A, Olaya MM, Reyes-Labarta JA. Comments on the correlation of vapor-liquid equilibrium (VLE) data in azeotropic ternary systems. *Fluid Phase Equilib*. 2016;426:110-118.
53. Renon H, Prausnitz JM. Local compositions in thermodynamic excess functions for liquid mixtures. *AIChE J*. 1968;14:135-144.
54. Treybal RE. *Liquid Extraction*. 2nd ed. McGraw-Hill; 1963.
55. Vicente-Martínez, M, Labarta, JA. Análisis topológico del modelo NRTL en sistemas binarios y ternarios para caracterizar la tipología de los sistemas líquido-líquido que predice en función de los valores de los parámetros de interacción binaria. Institutional Repository of the University of Alicante (RUA). 2021. http://hdl.handle.net/10045/117665.
56. Labarta JA, Olaya MM, Marcilla A. GMcal_TieLinesLL: Graphical User Interface (GUI) for the Topological Analysis of Calculated GM Surfaces and Curves, including Tie-Lines, Hessian Matrix, Spinodal Curve, Plait Point Location, etc. for Binary and Ternary LLE Data. Institutional Repository of the University of Alicante (RUA). 2015. http://hdl.handle.net/10045/51725.
57. Marcilla A, Reyes-Labarta JA, Serrano MD, Olaya MM. GE models and algorithms for condensed phase equilibrium data regression in ternary systems: limitations and proposals. *Open Thermodyn J*. 2011;5(Suppl 1-M5):48-62.
58. Sørensen JM, Artl W. Liquid-liquid equilibrium data collection. *Chemistry Data Series*. Vol. V/2. DECHEMA; 1980.
59. Labarta JA, Olaya MM, Marcilla A. Boundaries_LL_NRTL: graphical user interface (GUI) for the characterization of the NRTL model: Binary spinodal surfaces (in the $\tau_{i,j}$-$\tau_{j,i}$-x_i space), LLE maps and miscibility boundaries. Institutional Repository of the University of Alicante (RUA). 2022. http://hdl.handle.net/10045/121471.
60. Wang K, Al-Haimi AA, Zhang T, et al. Explorations of liquid-liquid phase equilibrium for the mixture (isopropanol + water) with Pyridinium-based ionic liquids. *J Chem Eng Data*. 2021;66(5):2192-2199.
61. Wang D, Wei F, Labarta JA, et al. Liquid-liquid equilibrium measurements and interaction explorations for separation of azeotrope n-butyl acetate and n-butanol using three ionic liquids. *J Chem Thermodyn*. 2021;155:106349-106354.
62. Zhang L, Bing X, Cui Z, et al. Multiscale exploration and experimental insights for effective separating representative neutral heterocyclic nitrogen compounds via [emim][NO_3] as extractant. *ACS Sustainable Chem Eng*. 2020;8(14):5662-5673.
63. Zhang X, Wang Z, Wang K, et al. Liquid-liquid phase equilibrium and interaction exploration for separation of azeotrope (2,2,3,3-tetrafluoro-1-propanol + water) with two imidazolium-based ionic liquids. *J Mol Liq*. 2020;300:112266-112273.
64. Rosenthal, RE. GAMS: General Algebraic Modelling System—A user's guide. 2016. https://www.gams.com.
65. Vecchietti A, Lee S, Grossmann IE. Modeling of discrete/continuous optimization problems: characterization and formulation of disjunctions and their relaxations. *Comput Chem Eng*. 2003;27:433-448.
66. Trespalacios F, Grossmann IE. Review of mixed-integer nonlinear and generalized disjunctive programming methods. *Chem Ing Tech*. 2014;86:991-1012.
67. Gmehling J, Menke J, Krafczyk J, Fischer K. *Azeotropic Data*. Wiley-VHC; 1994.

SUPPORTING INFORMATION

Additional supporting information can be found online in the Supporting Information section at the end of this article.

How to cite this article: Labarta JA, Olaya MM, Marcilla AF. What does the NRTL model look like? Determination of boundaries for different fluid phase equilibrium regions. *AIChE J*. 2022;68(10):e17805. doi:10.1002/aic.17805